

Electronic Supplementary Information

Experimental details

Material characterization. Powder X-ray diffraction (XRD) tests were run on a Bruker D8 Advance X-ray instrument (Cu $K_{\alpha 1}$ radiation = 1.5406 Å) with a voltage of 40 kV and a current of 40 mA. Field emission scanning electron microscopy (FESEM; Helios G4 CX) and transmission electron microscopy (TEM; JEOL, JEM-2010) were used to examine the morphology and structure of the samples. Component of the samples was determined using an inductively coupled plasma emission spectrometer (iCAP7400). X-ray photoelectron spectroscopy (XPS) analysis and UV photoelectron spectroscopy were done on a PHI Quantum 2000 XPS system with the C 1s binding energy (284.60 eV) as a reference and He I excitation (21.22 eV) as a monochromatic light source. The energy resolution of XPS analysis is set to 0.43 eV. N₂ adsorption-desorption isotherm characterization was carried out at Micromeritics ASAP3020 with 6 h degassing at 160 °C followed by N₂ adsorption-desorption characterization at liquid nitrogen temperature (77 K). The UV-Vis diffuse reflectance spectra (DRS) have been acquired with a Varian Cary 500 UV-Vis spectrometer equipped with an integrating sphere, using BaSO₄ as a reference. The photoluminescence (PL) properties were tested on a Hitachi F-7000 spectrophotometer at room temperature. Fluorescence lifetimes were measured by recording time-resolved fluorescence emission spectra on a Deltapro fluorescence lifetime system. A Nicolet IS50 FTIR spectrometer (Thermo SCIENTIFIC) to collect Fourier transform infrared (FTIR) spectra and in-situ Fourier transform infrared (in-situ DRIFTS) spectra were chosen.

Electrochemical analyses were performed on a Metrohm Autolab electrochemical system employing a conventional three-electrode system with a Pt electrode and an Ag/AgCl electrode as counter electrode and reference electrode. Typically, 10 mg of the sample was dispersed in N, N-dimethylformamide (1 mL) by sonication to obtain a homogeneous slurry. The obtained slurry is subsequently spread on the FTO glass over an area of approximately 0.25 cm². Transient photocurrent response spectra were

collected in aqueous Na_2SO_4 solution (0.20 M) with a 365 nm LED lamp as the light source. Electrochemical impedance spectroscopy (EIS) measurements were taken at open circuit potential. Electron paramagnetic resonance (EPR) signal was tested on a Bruker A.S.A. Under ambient conditions, a certain amount of photocatalyst was transferred into EPR tubes with a 365 nm LED lamp as the light source, and a certain amount of deionized water dissolved with methane gas or methanol was added, and DMPO was used as the trapping agent to determine $\cdot\text{CH}_3$ and $\cdot\text{O}_2^-$, respectively. The gases produced after the photocatalytic methane oxidation coupling reaction were analyzed and quantified at the Agilent 7890B gas chromatograph (GC). $^{13}\text{C}_2\text{H}_6$ experiments generated from $^{13}\text{CH}_4$ isotope experiments were detected by SHIMADZU gas chromatograph-mass spectrometer (GCMS-QP2020NX W/O RP).

Preparation of catalysts

$\text{Zn}_2\text{Ti}_3\text{O}_8$ nanospheres were prepared according to a modified solvothermal method¹. In a typical process, 10 mmol of $\text{Zn}(\text{CH}_3\text{COO})_2 \cdot 2\text{H}_2\text{O}$ were dissolved in 60 mL of ethylene glycol under mild stirring overnight. Then, 8 mmol of tetrabutyl titanate were added dropwise. After stirring for 30 min, the obtained uniform solution was transferred into a 100 mL Teflon-lined autoclave and kept in an oven at 180 °C for 24 h. After cooling down to room temperature, the precipitate was collected by centrifugation and then washed with ethanol and deionized water in order. Eventually, the dried precursor was ground well and annealed at 600 °C for 2 h in air to obtain $\text{Zn}_2\text{Ti}_3\text{O}_8$ nanospheres.

The Au nanoparticles were deposited on $\text{Zn}_2\text{Ti}_3\text{O}_8$ nanospheres via a simple NaBH_4 reduction method. Typically, 200 mg of $\text{Zn}_2\text{Ti}_3\text{O}_8$ nanospheres were homogeneously dispersed in 30 mL of deionized H_2O with magnetic stirring. Subsequently, 0.20 mL of 10 mg mL^{-1} of HAuCl_4 aqueous solution was added and stirred for 4 h to form a uniform dispersion, followed by the addition of 1 mL of 6 mg mL^{-1} NaBH_4 solution. After reaction for 15 min, the resultant sample was washed with deionized water and dried in an oven at 100 °C for 6 h. The obtained samples were recorded as 1.0%-Au/ $\text{Zn}_2\text{Ti}_3\text{O}_8$. The deposition of Au and other metal cocatalysts was similar to the procedure of preparing 1%-Au/ $\text{Zn}_2\text{Ti}_3\text{O}_8$, except changing the amount of metal precursor aqueous

solution (i.e., HAuCl₄, AgNO₃, Na₂PdCl₄, H₂PtCl₆ and RuCl₃).

Photocatalytic Methane Conversion.

Before the reaction, 30 mg of catalyst was loaded into a quartz disk with a diameter of about 30 mm, followed by the addition of 1 mL of H₂O in drops, which was then ultrasonicated to scatter the catalyst uniformly before transferring it to an oven at 100 °C for 20 min to form a catalyst film. In a batch glass reactor with a quartz window at the top, the quartz disk described above was placed in the middle of the reactor before CH₄ was introduced with O₂ to reach a pressure of 1 atm. Subsequently, the reactor was placed under a 365 nm LED lamp to react for 2 h. The gas products were analyzed and quantified by a gas chromatograph equipped with a thermal conductivity detector and a hydrogen flame ionization detector.

Determination of apparent quantum efficiency (AQE_{C₂H₆}).

AQE_{C₂H₆} was measured using a monochromatic light (365 nm) as the light source under the otherwise same reaction conditions. The light intensity was 0.27 W cm⁻² determined by an International light technology 950 spectroradiometer. The irradiation area was 0.25 cm² and reaction time was 1 h. After reaction, the yield of C₂H₆ was determined to be 3.91 μmol. The AQE_{C₂H₆} was calculated using the following equation:

$$\text{AQE}_{\text{C}_2\text{H}_6} = N_{\text{reacted}}/N_{\text{incident}} \times 100\% = 2MN_{\text{A}}hc/SPt\lambda \times 100\% = 1.05\%$$

Herein, N_{reacted} is the number of reacted electrons, N_{incident} is the number of used photons, M is the molecule of C₂H₆ (i.e., 3.91 × 10⁻⁶ mol), N_{A} is the Avogadro constant; h is the Planck constant; c is the speed of light; S is the irradiation area (0.25 cm²), P is the light intensity (0.27 W cm⁻²); t is the reaction time (3600 s); λ is the wavelength of incident light (3.65 × 10⁻⁷ m).

Determination of turnover number (TON).

$$\text{TON} = \frac{\text{Mole of C}_2\text{H}_6 \text{ molecules evolved}}{\text{Mole of Au sites}} = \frac{138.34 \mu\text{mol}}{0.58 \mu\text{mol}} = 239$$

The mole of Au sites is 0.58 μmol, which is determined by ICP-OES. The accumulated evolution of C₂H₆ in 8h stability tests are *ca.* 138.34 μmol, corresponding to a turnover

number (TON) of *ca.* 239 based on the Au sites (0.58 μmol), indicating the catalytic nature of the reaction.

The detailed calculation procedures for the UPS (Ultraviolet Photoelectron Spectroscopy) of $\text{Zn}_2\text{Ti}_3\text{O}_8$ are as follows:

The work function (ϕ) is calculated by Eq. (1): $\phi = h\nu - E_{\text{SEO}}$. Here, $h\nu$ (21.22 eV) represents the energy of monochromatic ionizing light, while E_{SEO} is the secondary electron onset obtained from the linear extrapolation of UPS spectrum.

The Fermi level (E_f) is obtained from work function by Eq. (2): $E_f = -\phi$. The valence band (VB) potential (E_{VB}) is obtained by Eq. (3): $E_{\text{VB}} = E_f - X$, in which X is obtained from the extrapolation of onsets of UPS spectrum. Therefore, the conduction band (CB) potential (E_{CB}) is obtained by Eq. (4): $E_{\text{CB}} = E_{\text{VB}} + E_g = E_f - X + E_g$. Here, E_g is the bandgap energy obtained by the Tauc plot.

All the potentials mentioned above refer to the vacuum energy. The vacuum energy (E_{vac}) in electronvolt (eV) can be converted to E (V vs. RHE) according to the formula between the reversible hydrogen electrode (RHE) and E_{vac} (i.e., $E_{\text{RHE}} = -E_{\text{vac}} - 4.44$). The potential of RHE equals to the normal hydrogen electrode (NHE) at pH = 0. Based on the relationship between RHE and NHE (i.e., $E_{\text{NHE}} = E_{\text{RHE}} - 0.0591\text{pH}$), the potential can be converted to E (V vs. NHE, pH = 7).

The work function of $\text{Zn}_2\text{Ti}_3\text{O}_8$ was determined as 3.54 eV (vs. E_{vac}), applying the method of linear approximation to the UPS spectrum to obtain the secondary electron onset (i.e., 17.28 eV vs. E_{vac} , Figure 3b). The Fermi level of $\text{Zn}_2\text{Ti}_3\text{O}_8$ was estimated as -3.54 eV (vs. E_{vac}). Simultaneously, E_{VB} of $\text{Zn}_2\text{Ti}_3\text{O}_8$ is calculated as -7.07 eV (vs. E_{vac}). According to the formula $E_{\text{RHE}} = -E_{\text{vac}} - 4.44$, E_{VB} of $\text{Zn}_2\text{Ti}_3\text{O}_8$ is determined as 3.05 V (vs. RHE), corresponding to 2.64 V (vs. NHE, pH = 7). Therefore, considering the bandgap energy of 3.60 eV, E_{CB} of $\text{Zn}_2\text{Ti}_3\text{O}_8$ is about -0.97 V (vs. NHE, pH = 7).

Determination of selectivity (S).

$$S = \frac{\sum x_n C_x H_y}{n_{CO_2} + \sum x_n C_x H_y} \times 100\%$$

The yields of each product (C₂H₄, C₂H₆, C₃H₆, C₃H₈, and CO₂) were 15.1, 609.5, 5.7, 50, and 103.8 μmol g⁻¹, respectively, after 2h illumination.

Table S1. Comparison of photocatalytic OCM performance of Au/Zn₂Ti₃O₈ with other reported catalysts under comparable conditions.

Catalyst	Reaction conditions	Light source	Main product and Sel. ($\mu\text{mol g}^{-1} \text{h}^{-1}$)	Ref.
Au/Zn ₂ Ti ₃ O ₈ (0.03 g)	CH ₄ : O ₂ = 15: 1, mild condition	λ = 365 nm 50 W LED	C ₂ H ₆ : 609.5 Sel.: 80%	This work
Au/ZnGa ₂ O ₄ (0.01 g)	CH ₄ : O ₂ = 4: 1.6	300 W Xe lamp	C ₂ H ₆ : 1315.3 Sel.: 53.3%	2
Cu _{0.1} Pt _{0.5} /PC-50 (0.1 g)	CH ₄ : O ₂ = 400 : 1, GHSV= 2400 h ⁻¹ , mild conditions	λ = 365 nm 40 W LED	C ₂ H ₆ : ~65 Sel.: 60%	3
6 wt%AgHPW/TiO ₂ (0.1 g)	CH ₄ and air, 0.3MPa	400 W Xe lamp	C ₂ H ₆ : ~20.6 Sel.: 90%	4
5 mol% Ce/Al ₂ O ₃ (0.2 g)	200 μmol CH ₄ , 27 °C	300 W Xe lamp	C ₂ H ₆ : 0.248	5
(Zn ⁺ , Zn ²⁺)-ZSM-5 (1 g)	200 μmol CH ₄ , 30 °C	150 W Hg lamp	C ₂ H ₆ : 2.93 Sel.: 99 %	6
Ga-ETS-10-0.2 (0.2 g)	200 μmol CH ₄ , 30 °C	150 W Hg lamp (λ <390 nm)	C ₂ H ₆ : 10.89	7
1.0AuZnO/TiO ₂ (4/1) (0.02 g)	CH ₄ : air = 69 : 1, mild conditions	300 W Xe lamp	C ₂ H ₆ : 5020 Sel.: 90%	8
1.0Au/ZnO (0.005 g)	CH ₄ : O ₂ = 99 : 1 mild conditions	λ = 365 nm 350 mW cm ⁻² LED	C ₂ -C ₄ :683.6 Sel.: 83%	9
Pt/TiO ₂ (0.075 g)	CH ₄ and water	254 nm UV lamps	C ₂ H ₆ : ~55.6 Sel.: 61.7%	10

Table S2. Corresponding vibrational frequencies of the possible species by *in-situ* DRIFTS.

Vibrational frequencies (cm ⁻¹)	Possible species
2367, 2326	CO ₂
1432	*OCH ₃
1375	*CH ₃
1300	CH ₄
1221	*COOH

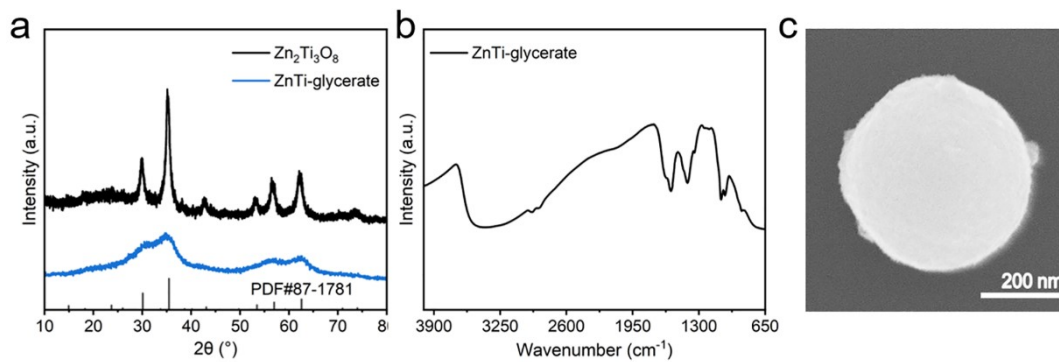


Figure S1. (a) XRD patterns, (b) FT-IR spectra and (c) SEM image of ZnTi-glycerate.

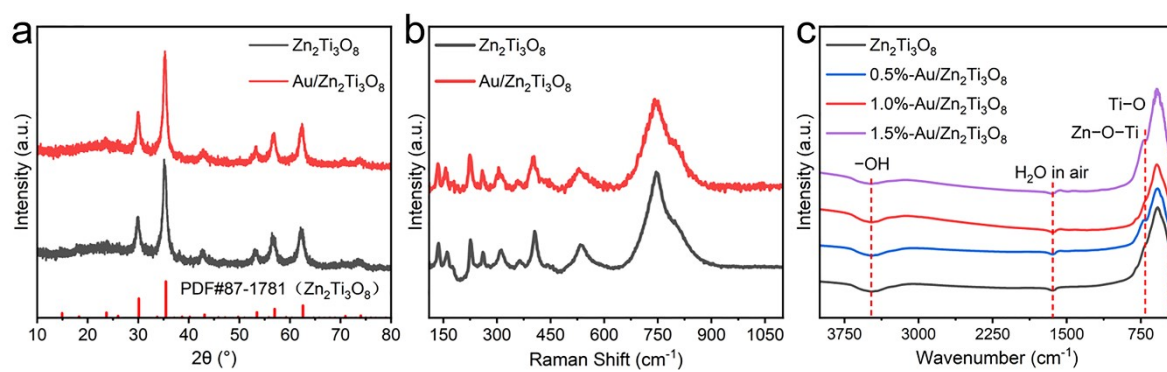


Figure S2. (a) XRD patterns, (b) Raman images and (c) FT-IR spectra of $Zn_2Ti_3O_8$ and Au/ $Zn_2Ti_3O_8$.

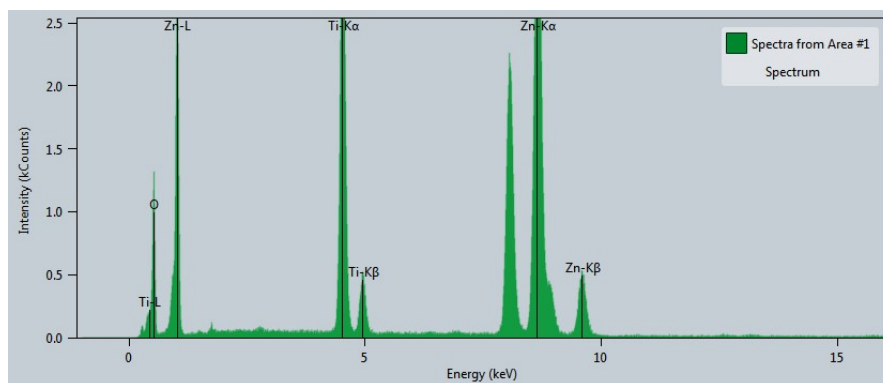


Figure S3. EDX spectrum of $\text{Zn}_2\text{Ti}_3\text{O}_8$.

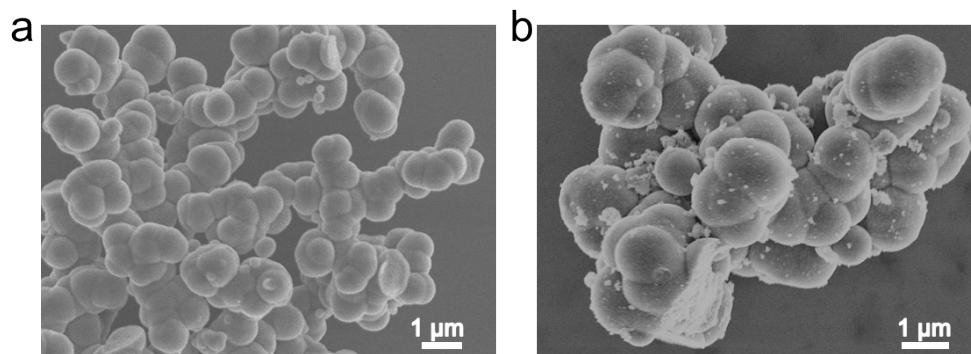


Figure S4. SEM images of (a) $\text{Zn}_2\text{Ti}_3\text{O}_8$ and (b) $\text{Au}/\text{Zn}_2\text{Ti}_3\text{O}_8$.

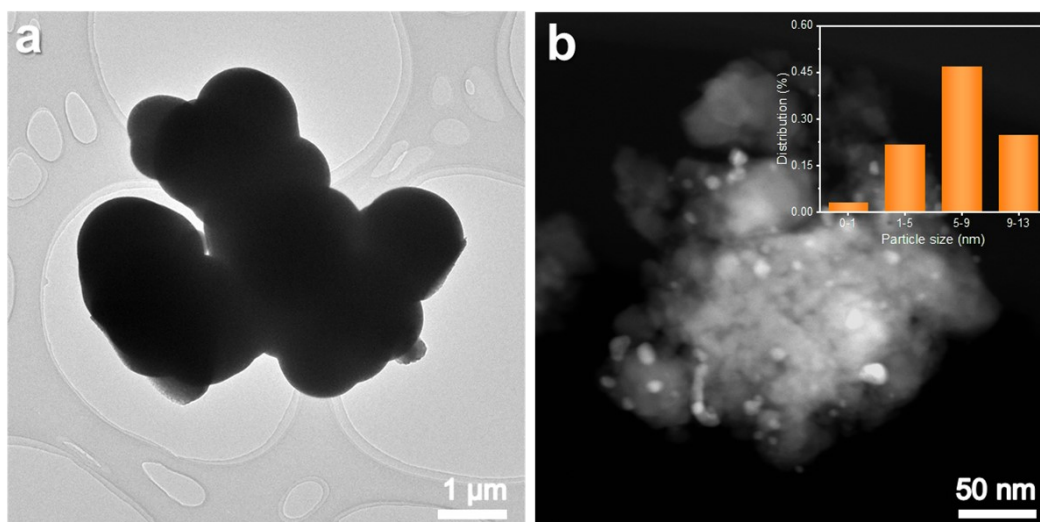


Figure S5. (a) TEM image of $\text{Zn}_2\text{Ti}_3\text{O}_8$. (b) TEM image of $\text{Au}/\text{Zn}_2\text{Ti}_3\text{O}_8$ and the particle size distribution of Au nanoparticles.

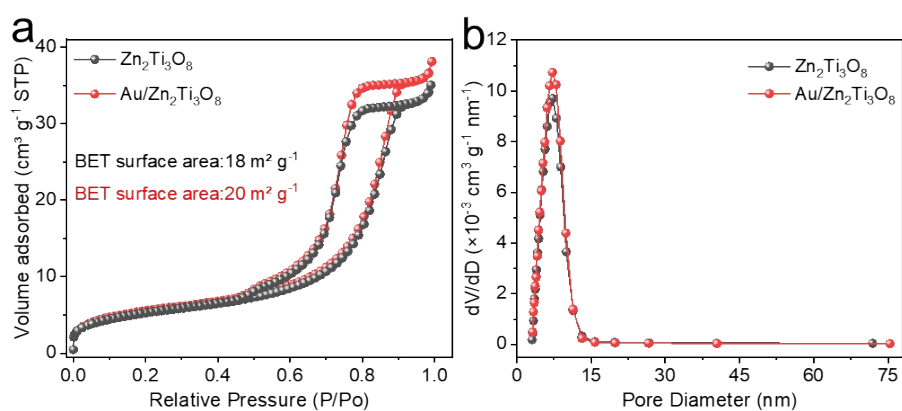


Figure S6. (a) N_2 adsorption-desorption isotherms and (b) the corresponding pore-size distribution curve of $\text{Zn}_2\text{Ti}_3\text{O}_8$ and $\text{Au}/\text{Zn}_2\text{Ti}_3\text{O}_8$.

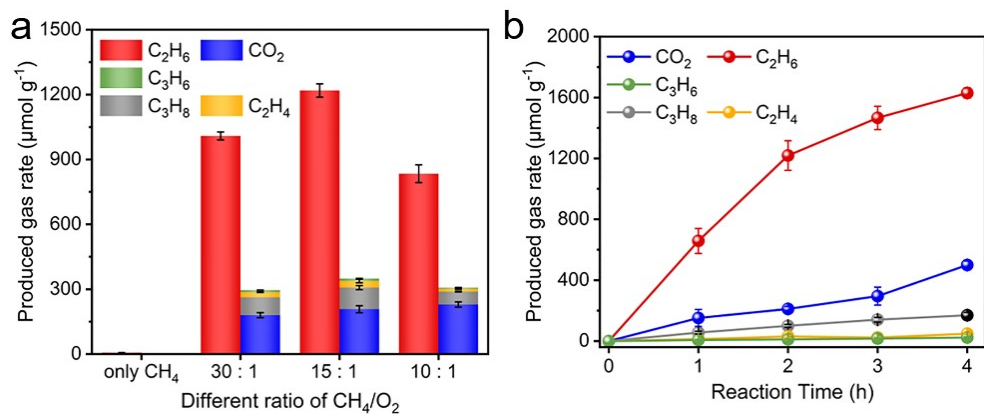


Figure S7. (a) Photocatalytic activity of OCM under different ratio of CH₄/O₂. (b) Photocatalytic activity of OCM over Au/Zn₂Ti₃O₈.

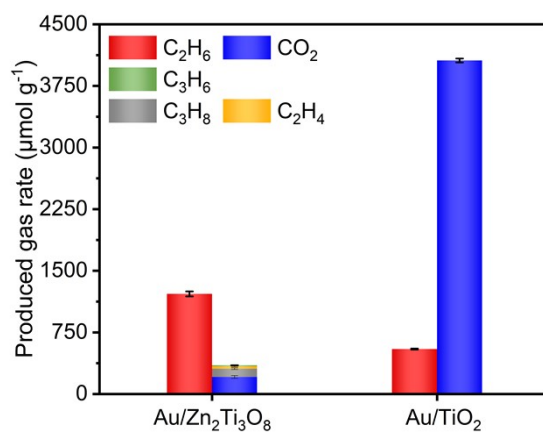


Figure S8. Photocatalytic OCM reaction performance of Au/Zn₂Ti₃O₈ and Au/TiO₂.

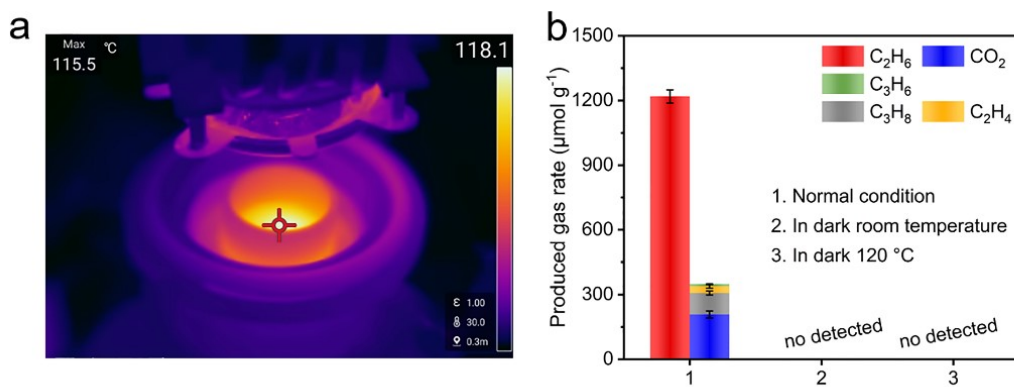


Figure S9. (a) The surface temperature of $\text{Au}/\text{Zn}_2\text{Ti}_3\text{O}_8$. (b) Photocatalytic OCM performance of $\text{Au}/\text{Zn}_2\text{Ti}_3\text{O}_8$ under different reaction conditions.

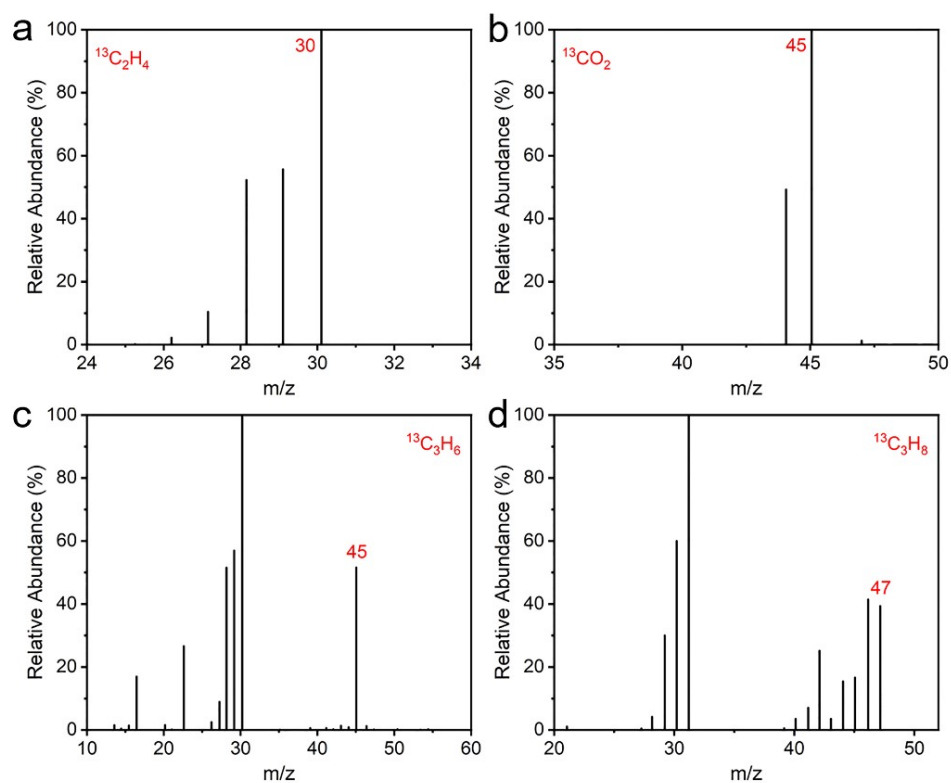


Figure S10. The $^{13}\text{CH}_4$ isotope results for (a) $^{13}\text{C}_2\text{H}_4$, (b) $^{13}\text{CO}_2$, (c) $^{13}\text{C}_3\text{H}_6$, (d) $^{13}\text{C}_3\text{H}_8$.

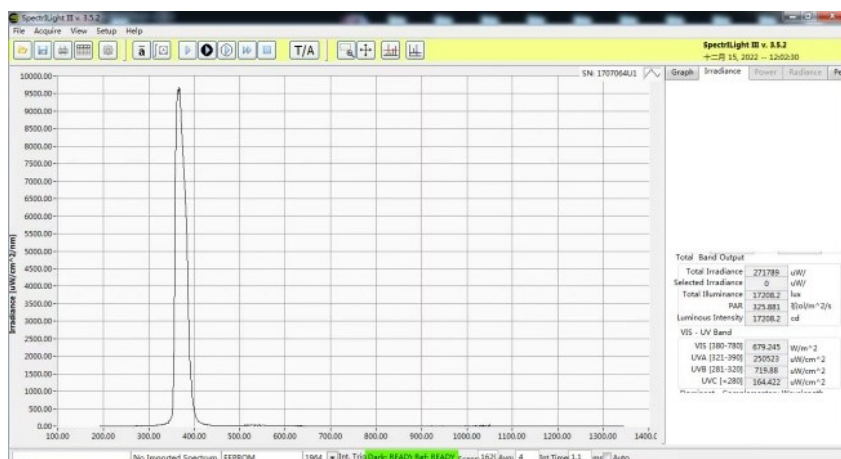


Figure S11. The light intensity of the LED lamp.

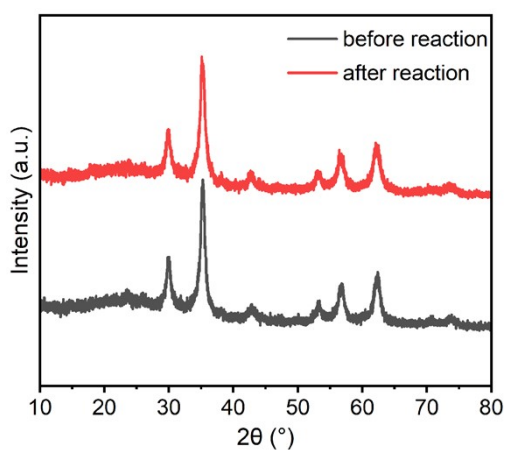


Figure S12. XRD patterns of Au/Zn₂Ti₃O₈ before and after reaction.

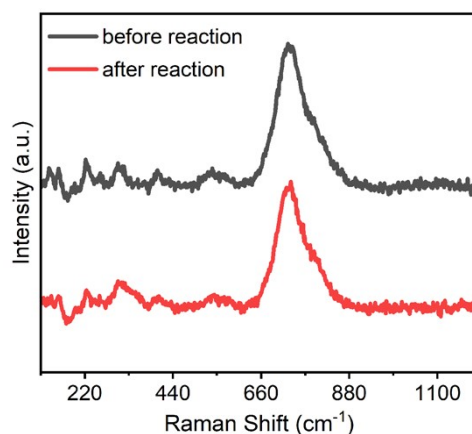


Figure S13. Raman spectra of Au/Zn₂Ti₃O₈ before and after reaction.

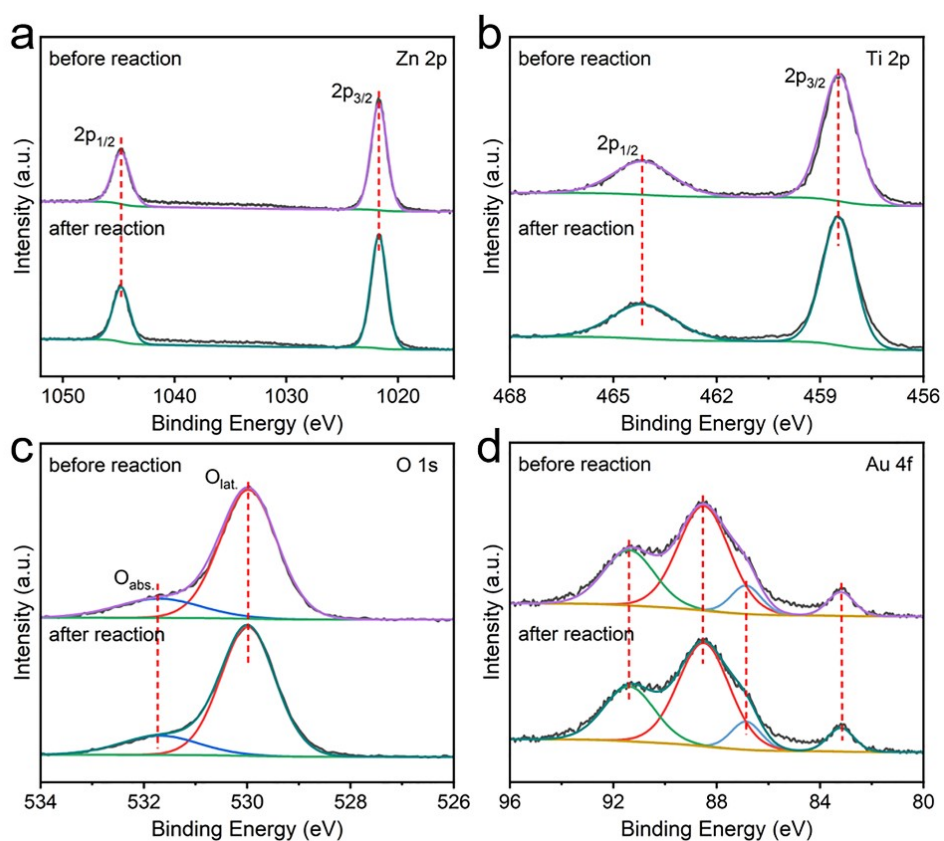


Figure S14. XPS spectra of Au/Zn₂Ti₃O₈ before and after reaction.

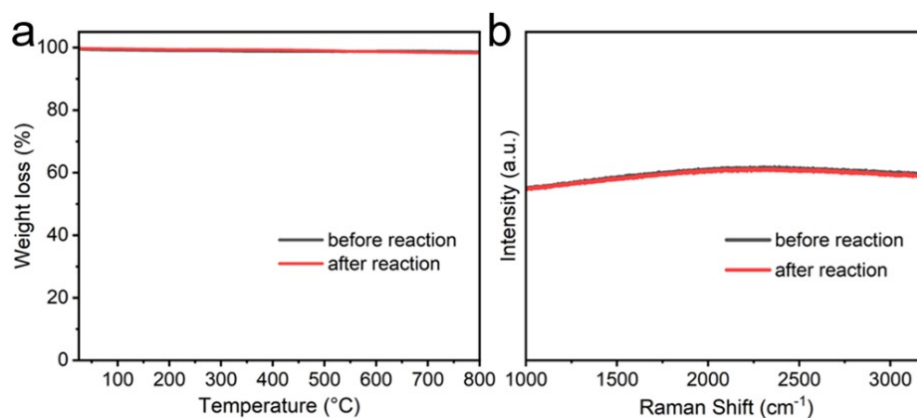


Figure S15. (a) TG profiles and (b) Raman spectra of Au/Zn₂Ti₃O₈ before and after reaction.

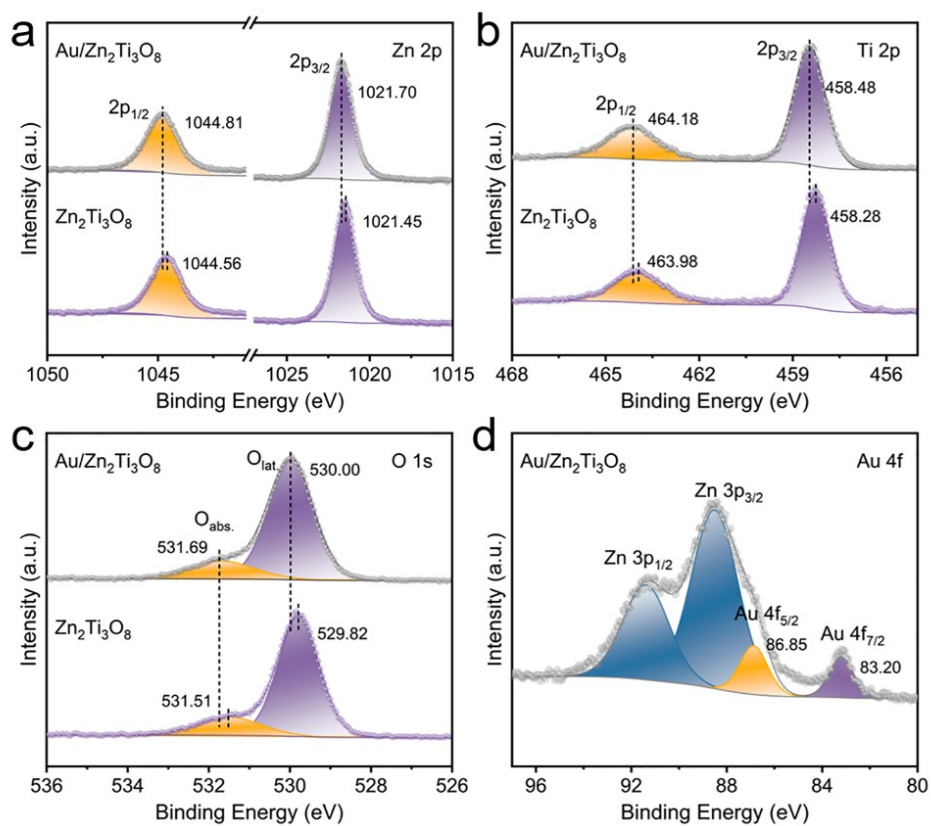


Figure S16. XPS spectra of Zn₂Ti₃O₈ and Au/Zn₂Ti₃O₈.

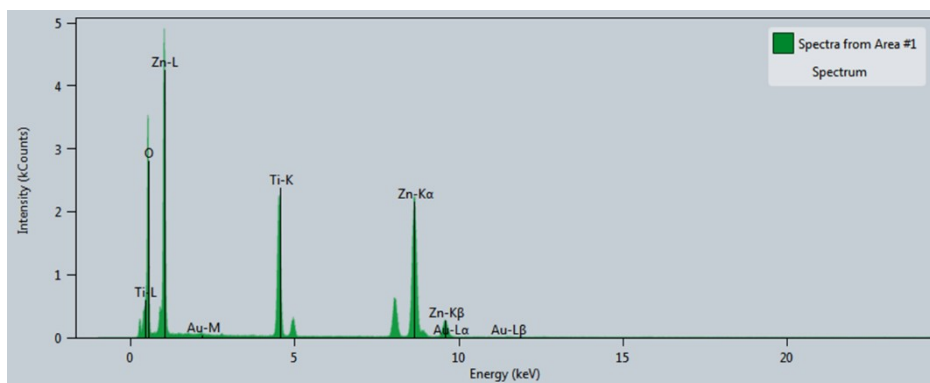


Figure S17. EDX spectrum of Au/Zn₂Ti₃O₈.

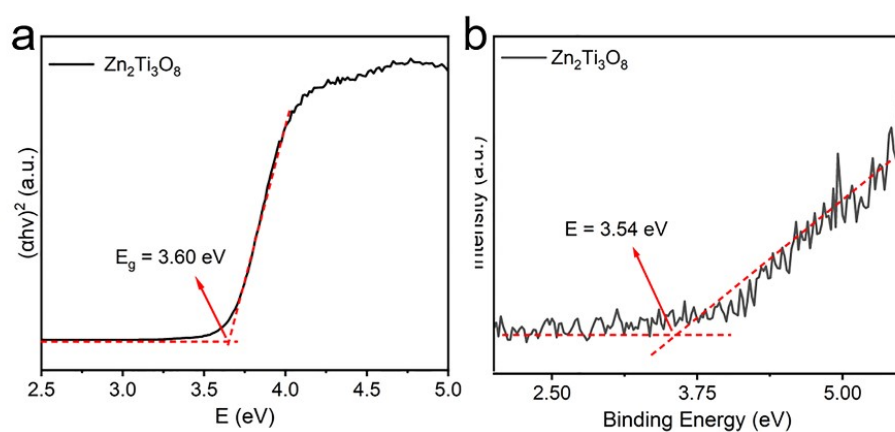


Figure S18. (a) Tauc plot of Zn₂Ti₃O₈. (b) UPS spectrum of Zn₂Ti₃O₈.

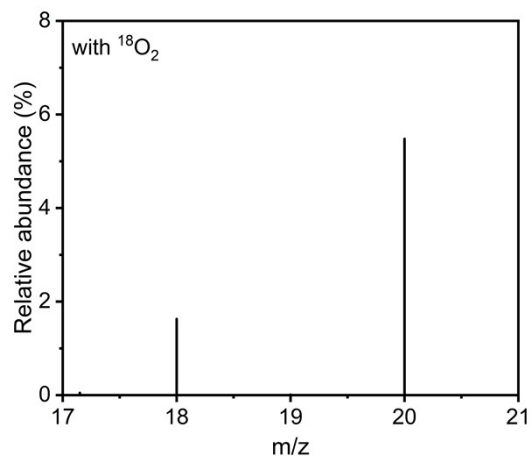


Figure S19. GC-MS result of the isotope labeling experiments in the presence of $^{12}\text{CH}_4$ and $^{18}\text{O}_2$.

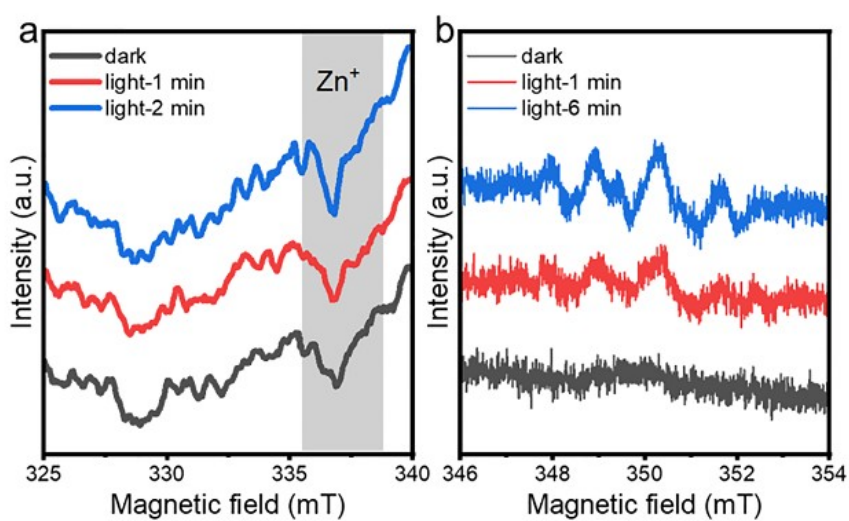


Figure S20. *In-situ* EPR spectra of $\text{Au}/\text{Zn}_2\text{Ti}_3\text{O}_8$ in dark and light.

References

1. C. Yu, F. Chen, D. Zeng, Y. Xie, W. Zhou, Z. Liu, L. Wei, K. Zheng and D. Li, *Nanoscale*, 2019, **11**, 7720-7733.
2. Y. Chai, S. Tang, Q. Wang, Q. Wu, J. Liang and L. Li, *Appl. Catal. B: Environ.*, 2023, **338**, 123012.
3. X. Li, J. Xie, H. Rao, C. Wang and J. Tang, *Angew. Chem. Int. Ed.*, 2020, **59**, 19702-19707.
4. X. Yu, V. L. Zholobenko, S. Moldovan, D. Hu, D. Wu, V. V. Ordonsky and A. Y. Khodakov, *Nat. Energy*, 2020, **5**, 511-519.
5. L. Yuliati, T. Hamajima, T. Hattori and H. Yoshida, *Chem. Commun.*, 2005, 4824.
6. L. Li, G. D. Li, C. Yan, X. Y. Mu, X. L. Pan, X. X. Zou, K. X. Wang and J. S. Chen, *Angew. Chem. Int. Ed.*, 2011, **50**, 8299-8303.
7. L. Li, Y. Y. Cai, G. D. Li, X. Y. Mu, K. X. Wang and J. S. Chen, *Angew. Chem. Int. Ed.*, 2012, **51**, 4702-4706.
8. S. Song, H. Song, L. Li, S. Wang, W. Chu, K. Peng, X. Meng, Q. Wang, B. Deng, Q. Liu, Z. Wang, Y. Weng, H. Hu, H. Lin, T. Kako and J. Ye, *Nat. Catal.*, 2021, **4**, 1032-1042.
9. P. Wang, R. Shi, Y. Zhao, Z. Li, J. Zhao, J. Zhao, G. I. N. Waterhouse, L. Z. Wu and T. Zhang, *Angew. Chem. Int. Ed.*, 2023, **62**, e202304301.
10. L. Yu, Y. Shao and D. Li, *Appl. Catal. B: Environ.*, 2017, **204**, 216-223.